SAR analysis of tri-band antennas for a 5G eyewear device

M. Dilruba Geyikoğlu[1] (iD), Hilal Koç Polat[2], Fatih Kaburcuk[3] and Bülent Çavuşoğlu[1]

[1]Electrical and Electronics Engineering, Ataturk University, Erzurum, Turkey; [2]Electrical and Electronics Engineering, Erzurum Technical University, Erzurum, Turkey and [3]Electrical and Electronics Engineering, Cumhuriyet University, Sivas, Turkey

Abstract

The goal of this study is to analyze the specific absorption rate (SAR) distribution of the projected 5G frequencies below 6 GHz and at Wi-Fi frequency (2.45 GHz) on a human head, for eyewear device applications. Two separate tri-band printed dipole antennas for this purpose are designed and fabricated at operating frequencies of 2.45/3.8/6 GHz for prototype-1 and at operating frequencies of 2.45/3.6/4.56 GHz for prototype-2. In order to obtain the desired frequencies: first, the prototypes of the proposed antennas are fine-tuned via Computer Simulation Technology Microwave Studio (CST) and then fabricated on the FR4 layer. The reflection coefficient (S_{11}) is tested and the simulation results are confirmed. In order to analyze the effect of wearing a pair of glasses' frame including a tri-band 5G antenna, a frame is designed and produced via 3D printer with polylactic acid material which has high dielectric constant ($\varepsilon_r = 8.1$). The SAR results of the proposed antennas have been examined for the cases where the antenna is embedded in the frame and is used alone. Both cases were analyzed by using the homogeneous specific anthropomorphic mannequin and the heterogeneous visible human head phantoms and the results have been evaluated in terms of $SAR_{10\,g}$ values.

Introduction

The use of personal wireless devices (smart phones, smart watches, smart glasses, etc.) operating at various frequencies has been gaining popularity. These devices have many applications such as navigation, driving assistance, video capture, and accept/reject incoming calls from a paired mobile phone. In addition to this, these devices developed for emerging technologies are expected to work with the Internet of Things (IoT) concept at 5G (fifth generation) frequencies [1, 2]. 5G frequencies in many countries have been determined, and the main band intervals identified are given in Table 1 (unlicensed band ranges are specified in bold, italic) [3, 4]. The frequencies subject to this study have been chosen so that they fall into these intervals.

The smart glasses are expected to replace smartphones with 5G technology in the near future [5, 6]. Since the 5G technology and IoT will cause more connected devices to be used, the time spent with smart devices tends to increase. Therefore, the usage time of smart glasses is expected to increase as well. Because of this situation, people may get more exposed to electromagnetic radiation compared to pre-IoT era and it may be dangerous to human health if the allowed standard values determined by the International Commission on Non-Ionizing Radiation Protection (ICRNIP) [7] are exceeded as it may cause undesired heating effects on the tissue [8]. Hence, it is important to know the specific absorption rate (SAR) distributions for these frequencies. However, the studies considering smart glasses in the literature, summarized in Table 2, have not made any SAR distribution analysis for the future 5G frequencies. There are some studies in the literature analyzing the SAR distributions of smart glasses on the head [9]. However, according to the authors' knowledge, this is the first study to examine SAR distributions in the frequencies of 2.45/3.6/3.8/4.56/6 GHz for smart glasses applications. In addition, while compact antenna structures of feasible sizes applicable on glasses are generally obtained by using coupling element structure in the literature, it has been obtained by using folded dipole and defected ground structure in this study.

In this study, the SAR distribution of the proposed tri-band antennas radiating at Wi-Fi and 5G frequencies integrated into the eyewear device has been investigated using two different human head models. The rest of the paper is organized as follows. In 'The feasibility study' section, first the prototype of 3D glasses considered as the frame of the smart glasses model is designed in CST Microwave Studio program and then fabricated. After that, the SAR distributions in the human head due to the proposed antennas integrated in the frame of the 3D glasses have been examined for the cases where the antenna is embedded in the frame and is used alone. Both cases have been analyzed by using the homogeneous specific

Table 1. The 5G frequency bands for various countries

Country	<1 GHz	<3 GHz	4 GHz	5 GHz	24–28 GHz	37–40 GHz	64–71 GHz
USA	600 MHz	2.5 GHz	**(3.55–3.7 GHz)** (3.7–4.52 GHz)	*(5.9–7.1 GHz)*	(24.25–28.35 GHz)	(37.6–42 GHz) (**47.2**–48.2 GHz)	**(64–71 GHz)**
Canada	600 MHz	–	–	–	(27.5–28.35 GHz)	(37–37.6 GHz) (**37.6**–40 GHz)	**(64–71 GHz)**
EU	700 MHz	–	3.4–3.8 GHz	*5.9–6.4 GHz*	(24.5–27.5 GHz)	–	–
China	–	–	3.3–3.6 GHz	4.8–5 GHz	(24.5–27.5 GHz)	(37.5–42.5 GHz)	–
Japan	–	–	3.6–4.2 GHz	4.4–4.9 GHz	(27.5–29.5 GHz)	–	–

anthropomorphic mannequin (SAM) and the heterogeneous visible human (VH) head phantoms. SAR values are evaluated based on international standards [7, 17]. In 'Fabricated prototypes' section, the fabrication of tri-band antenna prototypes and the production of 3D glasses are performed and these antennas have been evaluated in terms of reflection coefficients for their use in free space, in the glasses alone, and on the user's head with the glasses. Finally, in 'Conclusion' section, the effect of the proposed tri-band antennas on the SAR distribution and their maximum values on the head has been evaluated.

The feasibility study

In this section, design parameters and dimensions of the antennas, CST simulation results, and SAR distributions on the SAM phantom and VH phantoms are provided.

Design and analysis of antennas for eyewear devices model

In order to investigate the feasibility for different utilizations, many antennas operating at Wi-Fi and 5G frequencies are simulated and manufactured in [18–21]. However, printed dipole antenna is preferred for small-sized antennas due to its many advantages (easy to fabricate, simple, good gain, low profile, etc.) [20]. In this study, two printed dipole antennas are designed for 5G data communication. It is a challenging issue to combine all 5G frequencies in one antenna. Hence, in this study, we have provided two different antennas in order to be able to analyze wider range of frequencies and their SAR distributions on the head. In order to reduce the size of the antenna, the printed dipole antenna is meandered. The meanders are employed to implement a quarter of the wavelength of a dipole antenna; obvious size reduction for a dipole antenna can thus be achieved. The idea here is to reduce the size of the antenna by folding the conductors back and forth. However, while the antenna size decreases, radiation resistance, efficiency, and bandwidth decrease as well. These changes in antenna parameters also vary depending on the length, width, and number of the meanders [22]. With the help of empirical findings, antenna parameters are checked and the most suitable antenna design is proposed for the study. In the design of prototype-1 antenna for 2.45 GHz, a dipole antenna with 12.24 cm wavelength is utilized on the patch layer. The length of antenna is reduced by folding the dipole antenna from two separate points. In order to obtain a tri-band property, the effect of the ground layer is utilized. A circular space is constructed over the ground layer to shorten the electrical length. Two additional resonance frequencies in the projected 5G frequencies are obtained by carefully adjusting the radius of the circle. The designed

Table 2. Comparison between smart glasses studies in the literature and the proposed work

Antenna type	Bandwidth	Operating band	Multiband implementation
Monopole/ Loop[10]	2.32–2.35[a]	2.4 GHz WLAN	Yes (dual-band)
PIFA[11]	2.35–2.42[b]	2.4 GHz	No (single-band)
IFA[12]	2.43–2.48[b]	2.4 GHz	No (single-band)
Monopole[13]	2.28–2.62[b]	Bluetooth and Wi-Fi	No (single-band)
CE[14]	0.7–0.96/ 1.7–2.7[a]	LTE	Yes (dual-band)
Dual-CE[14]	0.7–0.96/ 1.7–2.7[a]	LTE	Yes (dual-band)
CE[15]	0.72–0.96/ 1.32–2.4[a]	LTE	Yes (dual-band)
CE[2]	0.7–2.7[a]	LTE	Yes (dual-band)
Loop[16]	0.81–1.07/ 1.68–2.7[a]	LTE	Yes (dual-band)
Printed dipole (our study)	2.42–2.56/ 3.6–3.9/ 5.9–6.3[b] 2.37–2.51/ 3.48–3.6/ 4.48–4.54[b]	Wi-Fi and 5G (below 6 GHz)	Yes (tri-band)

CE, coupling element.
[a]−6 dB Bandwith.
[b]−10 dB Bandwith.

antenna (Fig. 1(a)) has a tri-band property in which one of the frequencies is 2.45 GHz. In prototype-2, the number of foldings is increased together with the adjustments on the electrical length of the ground layer to obtain a tri-band property (Fig. 1(b)). Since microstrip feeding is used in both prototypes, both designs are performed by using the impedance matching of the main dipole antenna prior to the folding stage. Two different meander dipole antennas, shown in Fig. 1, are designed and printed on FR-4 substrate ($\varepsilon = 4.3$, tan $\delta = 0.025$, and height 1.3 mm) with the dimensions of $36 \times 88 \times 1.3$ mm^3 and $41.5 \times 40.8 \times 1.3$ mm^3 for prototype-1 and prototype-2, respectively.

The simulation and measurement results of the reflection coefficients (S_{11}) of the proposed antennas are shown in Fig. 2. The dashed and solid lines show the S_{11} of prototype-1 and prototype-2, respectively. It can be seen from Fig. 2 that prototype-1 provides BW ∼ 50 MHz at f_1 = 2.45 GHz, BW ∼ 140 MHz at f_2 = 3.8 GHz, BW ∼ 400 MHz at f_3 = 6 GHz, and
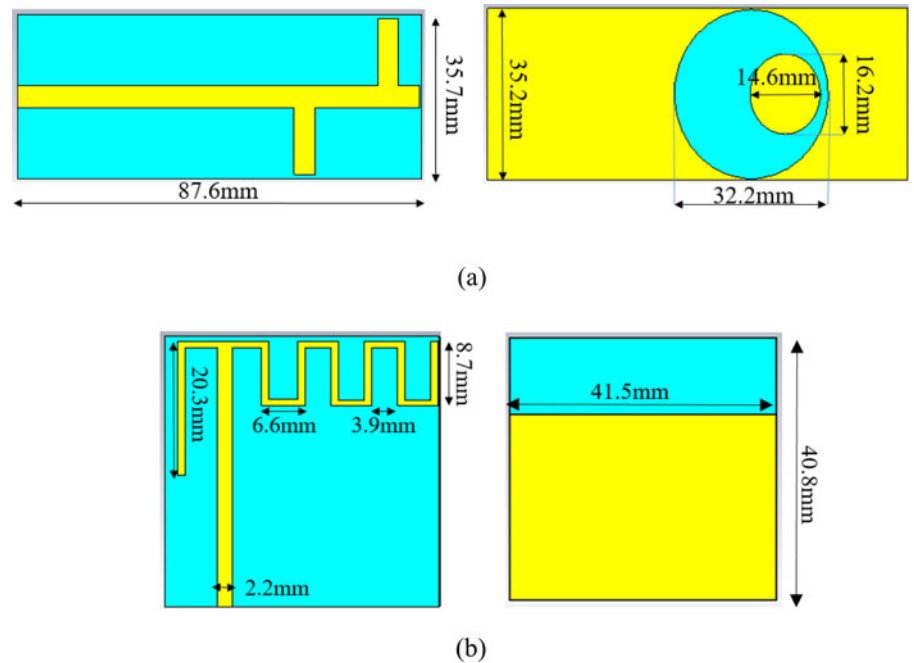
Fig. 1. The meander dipole antennas: (a) view of prototype-1 (left: top view, right: bottom view), (b) view of prototype-2 (left: top view, right: bottom view).
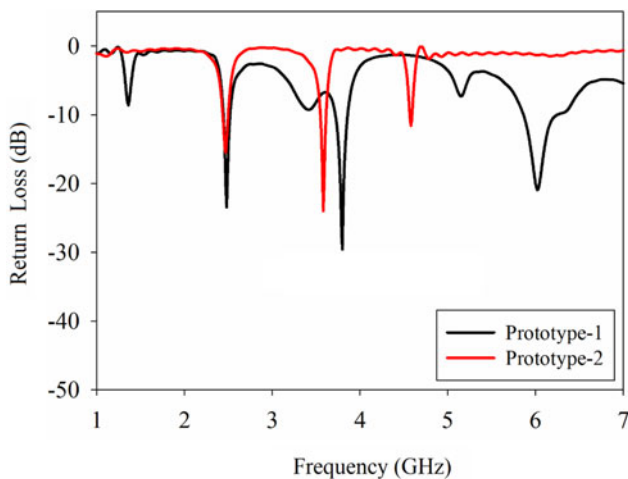

Fig. 2. S_{11} parameter of the simulated antennas for prototype-1 and prototype-2.

Fig. 3. Illustration of the simulated 3D glasses.

prototype-2 provides BW $\sim$ 100 MHz at f_1 = 2.45 GHz, BW $\sim$ 50 MHz at f_2 = 3.6 GHz, BW $\sim$ 40 MHz at f_3 = 4.56 GHz.

Design and analysis of 3D smart glass model with antennas

In this study, polylactic acid (PLA) material which has high dielectric constant (ε_r = 8.1) is preferred for the design of a 3D smart glass model shown in Fig. 3 in order to reduce the effects of the electromagnetic radiation from the antenna on the human head [23–25]. The electromagnetic properties and color of the PLA material are frequency dependent [26]. In order to place the antenna into the 3D smart glasses model, the right leg of the smart glasses has a cavity whose dimension is $85 \times 25 \times 2$ mm^3. The inner wall thickness of the 3D glasses, close to the user, is designed as 5 mm. During the use of the 3D glasses, a 2 mm-thick exterior wall is designed to protect the antenna against impacts. All dimensions of the smart glasses model are given in Fig. 3.
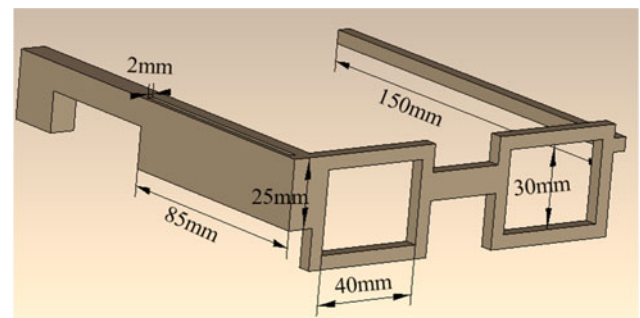
Homogeneous SAM and heterogeneous VH head phantoms provided in CST Microwave Studio Suite are used as the human head models in this study.

The 3D radiation patterns on the SAM head phantom obtained by placing all prototypes with glasses are shown in Fig. 4. All antennas are in the tendency to radiate in a direction perpendicular to the user's head as it is usually the case in smartphones.

SAR simulations

In the recent IEEE standard [17], the peak spatial-average SAR has been changed from 1 to 10 g of tissue in the shape of a cube [27]. Hence the evaluations are provided based on SAR$_{10\,g}$. The limits of SAR over any 10 g of tissue are determined by international standards [7, 17]. According to these standards, the average of SAR must be 2 W/kg over any 10 g of tissue (SAR$_{10\,g}$). The input power of the mobile devices can be adjusted to the appropriate level for the limiting of SAR. There are many studies [23, 24, 26] to obtain SAR distribution on the homogeneous SAM and heterogeneous VH head phantoms due to mobile devices. It is well known that the SAR values depend on the frequency
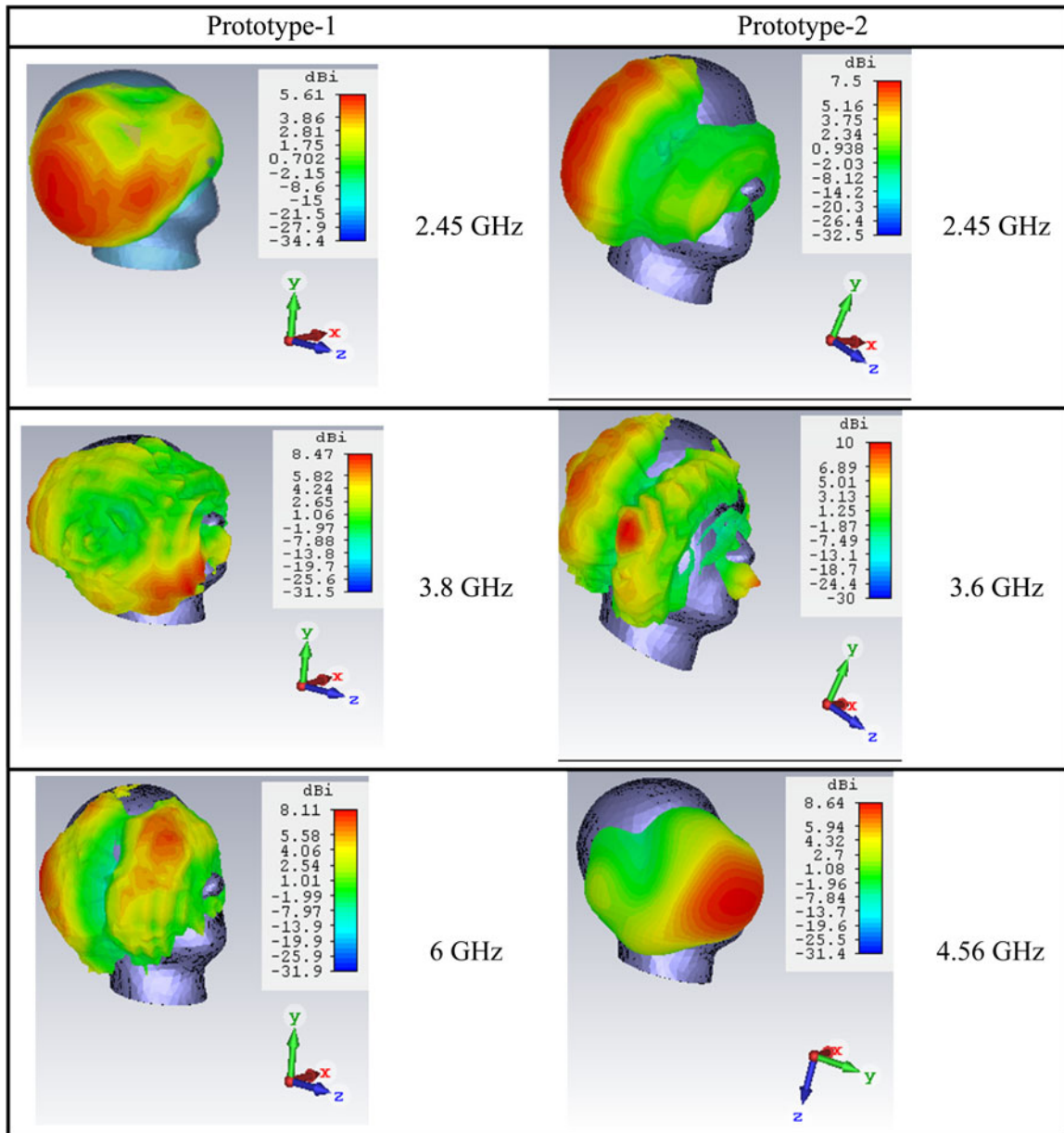
Fig. 4. 3D radiation patterns on the SAM head phantom obtained by placing all prototypes with glasses.
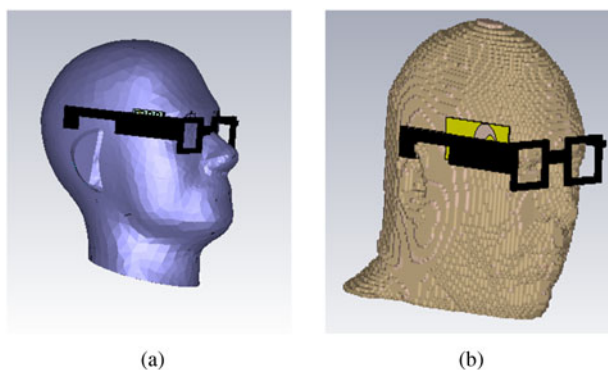

Fig. 5. The (a) SAM phantom and (b) VH phantom wearing the smart glasses model with the embedded antenna in the CST simulation environment.

Table 3. Simulated SAR values using SAM phantom (W/kg)

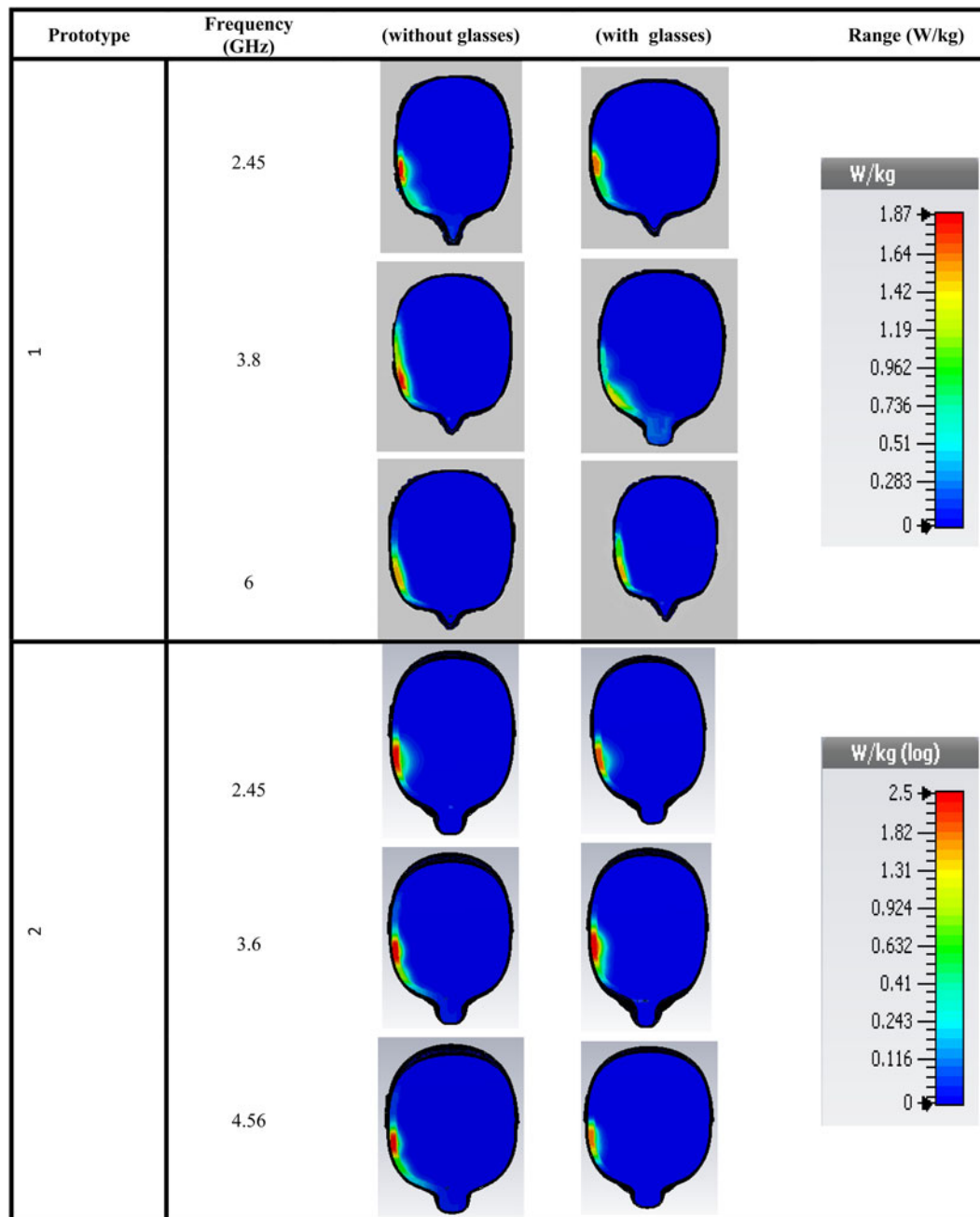| Prototype	Frequency (GHz)	10 g SAR(W/kg)	
		0.125W (without glasses)	0.125W (with glasses)
1	2.45	1.85	1.05
	3.8	1.08	0.83
	6	0.92	0.57
2	2.45	*2.48*	1.67
	3.6	1.82	1.32
	4.56	0.88	0.57

Fig. 6. $SAR_{10 g}$ distributions on the horizontal cross-section of the SAM phantom.

of interest due to the fact that the electromagnetic properties of the tissues depend on the frequency, antenna types, and distance between the human head and antenna. In this study, SAR values on the human head with and without 3D smart glasses model are calculated when the input power of the antenna is set to 0.125 W [28]. The SAM head and VH phantoms are provided in the library of CST Microwave Studio Suite. The SAM phantom and VH phantom wearing the smart glasses model with the embedded antenna in the CST simulation environment are shown in Fig. 5.

SAM phantom
The maximum $SAR_{10 g}$ values due to prototype-1 and prototype-2 are obtained for the SAM head phantom with and without the

Table 4. Simulated SAR values using VH phantom (W/KG)

		10 g SAR(W/kg)	
Prototype	Frequency (GHz)	0.125W (without glasses)	0.125W (with glasses)
1	2.45	0.87	0.72
	3.8	0.6	0.49
	6	0.48	0.29
2	2.45	1.73	1.17
	3.6	1.45	1.08
	4.56	0.44	0.35
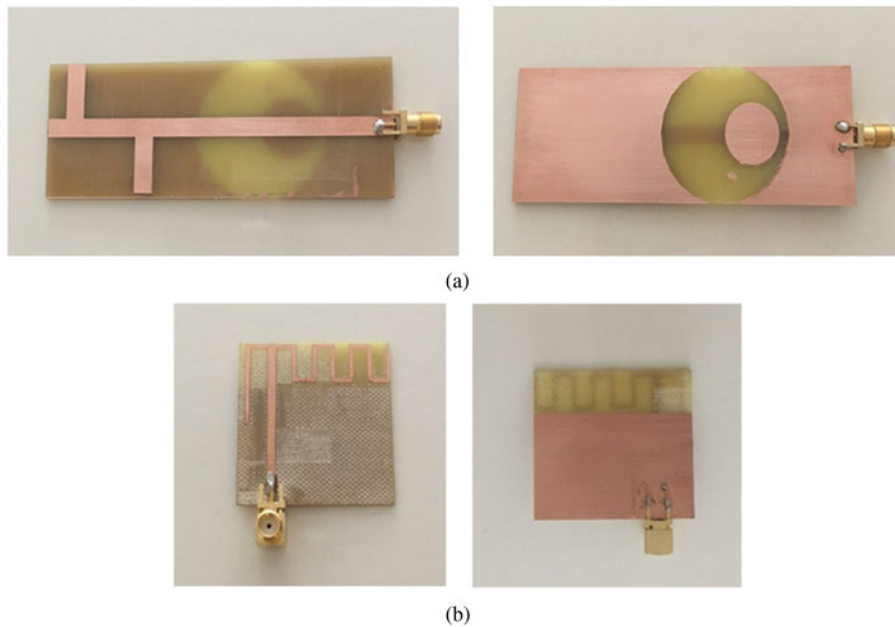
smart glasses and are given in Table 3. It is seen that the SAR values on the head decrease with increasing frequency. It is observed that wearing glasses causes lower SAR values. The efficiencies of the antennas also have a direct effect on the SAR values. The SAR values that exceed 2 W/kg are shown with bold and italic characters in the table. These SAR values can be reduced by decreasing the incident power.

The SAR_{10g} distributions on the horizontal cross-section of the SAM phantom are given in Fig. 6. It can be realized that the maximum SAR_{10g} values are decreasing when the antenna is embedded into the 3D glasses and also the SAR distributions are affected by the presence of the 3D glasses.

VH phantom

The maximum SAR_{10g} values for prototype-1 and prototype-2 are obtained for the VH phantom with and without the smart glasses model and are given in Table 4. It is realized that the maximum SAR_{10g} values obtained for the VH phantom are lower than those obtained for the SAM phantom. The reason for these differences in SAR values would be due to the fact that SAM and VH phantom model the head in different ways. SAM phantom uses an average electrical property of a single tissue, whereas VH phantom has a layered tissue structure [29].

Fabricated prototypes

In order to show the effect of the integrated antenna into the pair of eyewear devices operating at Wi-Fi and 5G frequencies on the human head, the prototypes of the 3D glasses and the embedded antennas were fabricated. The fabricated antennas are shown in Fig. 7.

The antennas are measured by using Agilent Technologies Network Analyzer N9928A in the frequency range of 300 kHz–26 GHz. The simulation and measurement reflection coefficients, shown in Fig. 8, for prototype-1 and prototype-2, are obtained in free space, the antenna without glasses placed next to the subject's head, and the antenna embedded in the glasses and worn by the subject. It can be realized that the reflection coefficients of the antennas are affected by the presence of the 3D glasses.

Different results between free space antenna measurements and simulations were observed both for prototype-1 and prototype-2, in terms of resonance frequency and reflection coefficients. It is believed that the difference between measurements and simulations may be due to the fact that there can be a difference between the assumed and real relative permittivity value of the substrate material.

For prototype-1 and prototype-2, when the antenna is not integrated into the 3D glasses model and placed alone next to the user's head without glasses, a shift is observed in the resonance frequencies and a few dB performance reductions are observed in the reflection coefficients, due to impedance mismatch caused by the tissues. However, when the antenna is integrated into the 3D glasses model and placed on the user's head with glasses, no change is observed in the resonance frequencies. In addition, for prototype-1, a new resonance frequency is formed (3.2 GHz). In the simulation, the SAM phantom is used as a human head model whereas a real human head is used in the measurement. The difference in resonance frequencies obtained in simulation and measurement is believed due to the fact that SAM phantom is used in the simulation and the real human head is used in the measurement.

Conclusion

In this study, SAR distributions of the projected 5G frequencies below 6 GHz and at Wi-Fi frequency (2.45 GHz) on a human head are analyzed, for eyewear device applications due to designed tri-band antennas. Two meandered dipole antennas operating at Wi-Fi and some 5G frequencies below 6 GHz are designed, simulated, and fabricated for smart glasses model. The 3D glasses model was fabricated using PLA material to investigate the possible effects of integrated antennas on the user's head.

The proposed antennas are placed into the right side of the 3D glasses. The maximum SAR_{10g} values in the VH and SAM
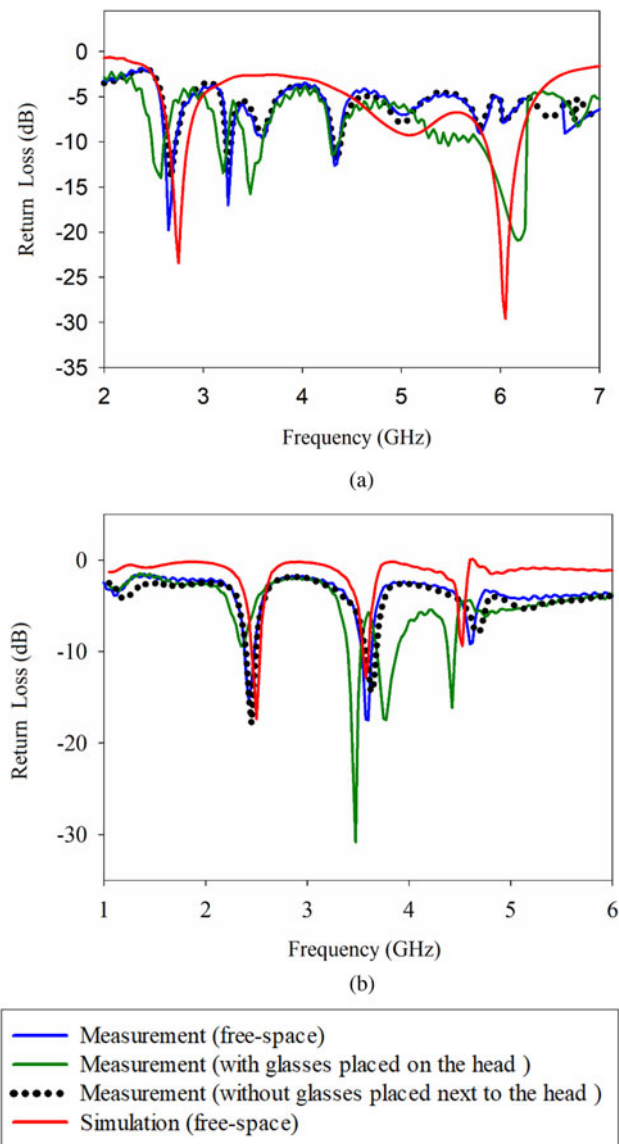
Fig. 8. Simulation and measurement results for prototype-1 and prototype-2 antennas.

phantom models are calculated based on two different antennas integrated into the eyewear devices. Thanks to the PLA material used in the fabrication of the 3D glasses, the amount of the electromagnetic radiation from the embedded antenna was reduced, and it was possible to obtain good SAR results. When the antennas are placed on the user's head without glasses, changes in resonance frequencies are observed due to the electrical properties of the tissues and even new frequencies are formed. However, when the antennas are placed on the user's head with the help of glasses, minimum changes are observed depending on the environmental factors in the antenna parameters (resonance frequency, reflection coefficient).

SAR distribution was not observed on other parts of the head away from the antenna as no current was induced on the frame used in this study due to its high dielectric value, while current distribution in different parts of the head has been observed in the studies carried out with metal glasses. However, secondary hotspots have been observed since the proposed antennas operate

at three different frequencies, thus causes current distribution in three different locations along the antenna.

This study helps to analyze the SAR distributions of several frequencies of 5G and the effects of the frame of glasses in terms of SAR distribution since the frames take the role of a protective shield for the head. It is realized that the 3D glasses have helped reduce the maximum SAR values compared to the case where the glasses are not used. As expected, the values of 10 g SAR values are higher in the tissues which are closer to the antenna in the head model. When the SAR values are normalized to the incident power 0.125 W, the 10 g SAR value calculated was below the allowed standard value. It can also be stated that, it is necessary to control the incident power because it is probable to go over the allowed standard SAR values as we have seen from the simulations.

References

1. **Lee Y-H, Wang A-S, Liao Y-D, Lin T-W, Chi Y-J, Wong C-C, Shinohara N, Yuan Q and Chen Q** (2017) Wireless power IoT system using polarization switch antenna as polling protocol for 5G mobile network. In *Wireless Power Transfer Conference* (*WPTC*), 2017 *IEEE*, IEEE, pp. 1–3.
2. **Cihangir A, Panagamuwa CJ, Whittow WG, Gianesello F and Luxey C** (2016) Ultrabroadband antenna with robustness to body detuning for 4G eyewear devices. *IEEE Antennas and Wireless Propagation Letters* **16**, 1225–1228.
3. **Pujol F, Manero C and Jaffal T** (2019) 5G Observatory Quarterly Report 4. **4**, 1-85. [Online]. Available at http://5gobservatory.eu/wp-content/uploads/2019/07/80082-5G-Observatory-Quarterly-report-4-min.pdf
4. **Kurka PRG and Salazar AAD** (2019) Applications of image processing in robotics and instrumentation. *Mechanical Systems and Signal Processing* **124**, 142–169. doi: 10.1016/j.ymssp.2019.01.015.
5. **Daponte P, De Vito L, Picariello F and Riccio M** (2013) State of the art and future developments of measurement applications on smartphones. *Measurement* **46**, 3291–3307.
6. **Ravikumar N, Metcalfe NH, Ravikumar J and Prasad R** (2016) Smartphone applications for providing ubiquitous healthcare over cloud with the advent of embeddable implants. *Wireless Personal Communications* **86**, 1439–1446.
7. **Guideline I** (1998) Guidelines for limiting exposure to time-varying electric, magnetic, and electromagnetic fields (up to 300 GHz). *Health Physics* **74**, 494–522.
8. **Mertz L** (2016) Are wearables safe?: we carry our smart devices with us everywhere-even to bed-but have we been sleeping with the enemy, or are cautionary tales overinflated? *IEEE Pulse* **7**, 39–43.
9. **Kaburcuk F and Elsherbeni AZ** (2018) Smart glasses radiation effects on a human head model at Wi-Fi and 5G cellular frequencies. In *2018 International Applied Computational Electromagnetics Society Symposium-China* (*ACES*), IEEE, pp. 1–2.
10. **Cihangir A, Gianesello F and Luxey C** (2018) Dual-antenna concept with complementary radiation patterns for eyewear applications. *IEEE Transactions on Antennas and Propagation* **66**, 3056–3063.
11. **Zheng Y-F, Sun G-H, Huang Q-K, Wong S-W and Zheng L-S** (2016) Wearable PIFA antenna for smart glasses application. In *2016 IEEE International Conference on Computational Electromagnetics (ICCEM)*, IEEE, pp. 370–372.
12. **Choi S and Choi J** (2017) Miniaturized MIMO antenna with a high isolation for smart glasses. In *2017 IEEE-APS Topical Conference on Antennas and Propagation in Wireless Communications (APWC)*, IEEE, pp. 61–63.
13. **Hong S, Kang SH, Kim Y and Jung CW** (2016) Transparent and flexible antenna for wearable glasses applications. *IEEE Transactions on Antennas and Propagation* **64**, 2797–2804.
14. **Cihangir A, Whittow WG, Panagamuwa CJ, Ferrero F, Jacquemod G, Gianesello F and Luxey C** (2013) Feasibility study of 4G cellular antennas

for eyewear communicating devices. *IEEE Antennas and Wireless Propagation Letters* **12**, 1704–1707.

15. **Cihangir A, Panagamuwa CJ, Whittow WG, Jacquemod G, Gianesello F, Pilard R and Luxey C** (2017) Dual-band 4G eyewear antenna and SAR implications. *IEEE Transactions on Antennas and Propagation* **65**, 2085–2089.

16. **Wang Y-Y, Ban Y-L and Nie Z** (2019) Dual-loop antenna for 4G LTE MIMO smart glasses applications. *IEEE Antennas and Wireless Propagation Letters* **18**, 1818–1822.

17. **IEEE** (2013) *IEEE Std. 1528-2013 recommended practice fordetermining the peak spatial-average specific absorptionrate (SAR) in the human head from wireless communica-tions devices—measurement techniques*. New York: Institute of Electrical and Electronics Engineers, pp. 1–246.

18. **Zhu J, Antoniades MA and Eleftheriades GV** (2010) A compact tri-band monopole antenna with single-cell metamaterial loading. *IEEE Transactions on Antennas and Propagation* **58**, 1031–1038.

19. **Ur-Rehman M, Adekanye M and Chattha HT** (2018) Tri-band millimetre-wave antenna for body-centric networks. *Nano Communication Networks* **18**, 72–81.

20. **Abu M, Rahim MKA, Suaidi M, Ibrahim I and Nor N** (2009) A meandered triple-band printed dipole antenna for RFID. In *Microwave Conference, 2009. APMC 2009. Asia Pacific*, IEEE, pp. 1958–1961.

21. **Fang X, Wen G, Inserra D, Huang Y and Li J** (2018) Compact wideband CPW-fed meandered-slot antenna with slotted Y-shaped central element for Wi-Fi, WiMAX, and 5G applications. *IEEE Transactions on Antennas and Propagation* **66**, 7395–7399.

22. **Bedir Yousif MS and Abdelrazzak M** (2015) Design and simulation of meander line antenna for LTE communications based on defected ground structure. *Ciência e Técnica Vitivinícola* **30**, 15–29.

23. **Hong Y and Choi J** (2018) 60 GHz Patch antenna array with parasitic elements for smart glasses. *IEEE Antennas and Wireless Propagation Letters* **17**, 1252–1256.

24. **Hwang J-N and Chen F-C** (2006) Reduction of the peak SAR in the human head with metamaterials. *IEEE Transactions on Antennas and Propagation* **54**, 3763–3770.

25. **Kaburcuk F and Elsherbeni AZ** (2018) Temperature rise and SAR distribution at wide range of frequencies in a human head due to an antenna radiation. *ACES Journal* **33**, 367–372.

26. **Hadjem A, Lautru D, Dale C, Wong MF, Hanna VF and Wiart J** (2005) Study of specific absorption rate (SAR) induced in two child head models and in adult heads using mobile phones. *IEEE Transactions on Microwave Theory and Techniques* **53**, 4–11.

27. **Kaburcuk F** (2019) Effects of a brain tumor in a dispersive human head on SAR and temperature rise distributions due to RF sources at 4G and 5G frequencies. *Electromagnetic Biology and Medicine* **38**, 168–176.

28. **Siegbahn M, Bit-Babik G, Keshvari J, Christ A, Derat B, Monebhurrun V, Penney C, Vogel M and Wittig T** (2010) An international interlaboratory comparison of mobile phone SAR calculation with CAD-based models. *IEEE Transactions on Electromagnetic Compatibility* **52**, 804–811.

29. **Kuster N, Christ A, Chavannes N, Nikoloski N and Frohlich J** (2002) Human head phantoms for compliance and communication performance testing of MTE. 2002 Interim International Symposium on Antennas and Propagation, Yokosuka Reserach Park, Japan November 26–28, 2002
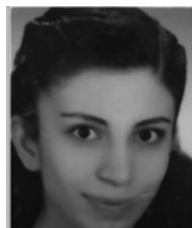
Miraç Dilruba Geyikoğlu received the B.S. degree in electrical and electronics engineering from Ataturk University, Erzurum, Turkey, in 2013, the M.S. degree from the Ataturk University, Erzurum, Turkey, in 2015. She is still a Ph.D. student from Ataturk University, Erzurum, Turkey. Her research interest includes the areas of antenna theory, bio-electromagnetics, and hyperthermia.

Hilal Koç Polat received the B.S. degree in electrical and electronics engineering from Ataturk University, Erzurum, Turkey, in 2013, the M.S. degree from the Ataturk University, Erzurum, Turkey, in 2015. She is still a Ph.D. student from Ataturk University, Erzurum, Turkey. She has been serving as a research assistant at the Department of Electrical and Electronics Engineering at Erzurum Technical University Erzurum, Turkey, since 2014. Her research interest includes the areas of signal processing, antenna theory, and wireless communication.

Fatih Kaburcuk received both the M.Sc. and Ph.D. degrees in electrical engineering from Syracuse University, Syracuse, New York, USA, in 2011 and 2014, respectively. He was a visiting research scholar in the Electrical Engineering Department at Colorado School of Mines in 2014. He was with the Erzurum Technical University in Turkey from 2015 to 2019. He joined the Electrical and Electronics Engineering Department at Sivas Cumhuriyet University in June 2019 as the Assistant Professor. His research interest includes numerical methods in electromagnetics, bioelectromagnetic, and microwave systems.

Bülent Çavuşoğlu received the B.S. degree in electrical and communication engineering from Yildiz Technical University, İstanbul, Turkey, in 1994, the M.S. degree from the Illinois Institute of Technology, Chicago, IL, USA in 1997, and the Ph.D. degree from the University of Illinois at Chicago, Chicago, in 2005, both in electrical and computer engineering. His research interest includes the areas of image/video processing, multimedia compression, multimedia communication networks, nanomolecular communication and sensors for chemical/biological molecules, and antenna theory.